hv photonics

IMPACT FACTOR 2.4

CITESCORE 2.3

Communication

Compact Design for Bi-Polarization Quantum Routers on SOI Platform

Zijie Dai, Eryi Pan, Xuefeng Chen, Xiaoxian Song, Haiting Zhang and Ying Liang

Special Issue

Recent Advances in Micro-Nano Optics

Edited by

Dr. Xiaodong Shi, Dr. Zhenyu Li, Dr. Fan Yang, Dr. Jingjing Zhang and Dr. Xiaorui Liang

MDPI

https://doi.org/10.3390/photonics10080897

photonics

MDPI

Communication

Compact Design for Bi-Polarization Quantum Routers on SOI Platform

Zijie Dai [1,2], Eryi Pan [1,2], Xuefeng Chen [1,2], Xiaoxian Song [1,2], Haiting Zhang [1,2] and Ying Liang [1,2,*]

[1] Institute of Mirco/Nano Optoelectronic and Terahertz Technology, Jiangsu University, Zhenjiang 212013, China
[2] School of Mechanical Engineering, Jiangsu University, Zhenjiang 212013, China
* Correspondence: 1000005989@ujs.edu.cn

Abstract: An ultra-compact optical quantum router (QR) consisting of a Mach–Zehnder interferometer (MZI) and waveguide tapers is proposed and numerically simulated, using silicon-on-insulator (SOI). The interferometer is designed to work at the center wavelength of 1550 nm with visibilities of 99.65% and 98.80% for TE and TM polarizations, respectively. Using the principle of phase compensation and self-image, the length of the waveguide tapers is shortened by an order of magnitude with the transmission above 95% for both TE and TM polarizations. Furthermore, polarization beam splitters (PBS) with an ultra-compact footprint of 1.4 × 10.4 μm^2 with transmissions of 98% for bi-polarizations are achieved by introducing anisotropic metamaterials. The simulated results indicate that the interferometer facilitates low loss, a broad operating spectral range, and a large tolerance to size variation in fabrications. The optical switch possesses the routing function while maintaining the polarization states, which promises to pave the point-to-point BB84 protocol into applications of network-based quantum communication.

Keywords: quantum router; polarization beams splitters; integrated photonics; silicon-on-insulator

Citation: Dai, Z.; Pan, E.; Chen, X.; Song, X.; Zhang, H.; Liang, Y. Compact Design for Bi-Polarization Quantum Routers on SOI Platform. *Photonics* **2023**, *10*, 897. https://doi.org/10.3390/photonics10080897

Received: 17 May 2023
Revised: 18 July 2023
Accepted: 1 August 2023
Published: 3 August 2023

1. Introduction

Quantum information processing technology has rapidly developed from a proof-to-concept to commercial applications [1,2]. Compared with classical optical information systems, quantum communication networks promise to be one of the feasible pathways towards fast-speed quantum information processing [3,4]. The quantum communication network is a complex information network composed of quantum channels and quantum notes, which provides the ultimate solution for the scalability of quantum computing and communication [5]. With the increase in computation and communication users, the bulk optical devices bolted onto optical tables in free space and fiber systems confine the development of the quantum communication networks towards chip-scale applications [6]. Therefore, integrated photonic circuits with low power consumption and potentially low-cost optoelectronic integration have become a next-generation platform for quantum communication networks. Although quantum photonic circuits on $LiNO_3$, InP and SiN platforms have been demonstrated [7–10], these waveguide materials with low refractive index contrast associated with large footprints and poor scalability bring challenges to large-scale quantum computing, high dimensional quantum communication and precision sensing.

Silicon-on-insulators (SOIs), with the advantages of compatibility with the complementary metal oxide semiconductor (CMOS) and strong confinement of light, allow for scalability, high-density integration and hybrid integration methods for integrated quantum photonic circuits [11]. As a node in a quantum network, quantum routers (QRs) are used to connect different quantum channels and quantum networks, as well as to select the path in the process of quantum information transmission [12]. At the same time, the transmitted quantum state must be kept constant, which requires photons to be carried

without destroying the information [13]. Therefore, the performance of quantum routers is the key factor affecting the future construction of large-scale quantum networks in the SOI platform. Recently, research on quantum routers has led to a multitude of theoretical and experimental observations based on various physical schemes, such as cavity quantum routers [14], superconducting routers [15] and quantum dots routers [16]. Most QRs can only route single photons or quantum entanglement states between few quantum channels. To realize a quantum information network, QRs should possess several intrinsic requirements such as being multi-user and scalable and having a small footprint [17]. A Mach–Zehnder interferometer (MZI) as well as a phase modulator in one path can work as the basic QR element to build multi-user quantum networks [18] by combing combining several devices across *N* paths and routing the photon from arbitrary paths. D.B et al. proposed an MZI interferometer composed of two multimode interferometers (MMI), which realizes quantum interference and the manipulation of entanglement in the silicon platform. The MZI-based QR is widely used in quantum key distribution (QKD) [19], quantum internet [20], multi-photon entanglement [21], quantum walking [22] and high-dimensional quantum entanglement [23]. In these demonstrations, the visibility of the MMI is limited to 80% for TE polarization, which significantly lowers the accuracy of quantum cryptography.

On the other hand, silicon waveguide devices are generally polarization sensitive, which would introduce polarization-dependent loss [23]. Since the polarizations are important freedom degrees of quantum coding, the polarization dependence of silicon waveguide devices brings intrinsic difficulties to demonstrating the large-scale computing schemes and quantum communication because the QRs can only manipulate photons with same polarization [24]. In 2016, J. Wang et al. firstly reported quantum photonic interconnection using an SOI platform, demonstrating high-fidelity entanglement distribution and manipulation between two separate photonic chips. However, the conversion between the path and polarization can only be distributed between the chip path and the fiber path. This shows that the quantum internet is difficult to realize as a monolithic integration for large-scale quantum computing architectures and systems application [25]. The limitations in quantum communication applications are also significant: for example, the loss of polarizations of freedom makes it hard for the silicon waveguide path system to realize the point-to-point BB84 QKD, which is the key technology of quantum security communication [26]. Z. Tong et al. reported a silicon photonic transmitter for polarization-encoded QKD, where the polarization modulators are used for TM\TE polarization conversion, while controlling one state of polarization and the polarization modulators introducing additional insertion loss are not applicable to the BB84-based QKD network [27]. In addition, the silicon quantum network can be used to realize a time–energy entanglement coding system [20], and long-distance transmission is required for decoherence due to its robustness, leading to a certain scale of the chip-based quantum network. Therefore, solving the polarization dependence problem of silicon-based QRs is an important step to realizing BB84-based quantum communication networks and large-scale quantum computing. In addition, to solve the mismatch between the input field from the fiber-adapted grating couplers and the single mode waveguide, a waveguide taper with a length over 400 μm is usually adopted. The large footprint decreases the compact of the photonic integrated circuit, which is unsuitable for a multi-user quantum information network [28]. Thus, the polarization dependence and lager footprint of the input/output signal should be considered in the related research.

In this paper, we propose an MZI-based active bi-polarization QR which can route single photon states and entangled photon pairs while maintaining the polarization of quantum states. A compact waveguide taper possessing a length of 27 μm is well-designed using a ladder-shaped waveguide taper and multimode waveguide, which enables a relatively high transmission of more than 95% for both TE and TM polarizations and significantly improves the integration of the photonics integrated circuits. The beam splitters reduce the risk of losing photons and ensure that photons equiprobably propagate along two channels in Ch1/Ch2 with the transmissions of 49.87%/49.81% and 49.07%/49.06% for TE

and TM polarizations, respectively. A PBS based on the anisotropic metamaterial structure are used for multiplexing and de-multiplexing the TM polarization [10]. By adjusting the corresponding path of the phase shifters, TE and TM polarizations can be output from an arbitrary port. The footprint of the optimized PBS is 1.4 × 10.4 μm^2, and a transmission of 98% is achieved for both polarizations. By interconverting between path and polarization degrees of freedom, path-entangled states are generated and distributed to the arbitrary user via the proposed QR on the same chip. The proposed structure holds great potential to realize network-based quantum communication following the BB84 protocol.

2. Design and Analysis

A schematic of the design interferometer structure is shown in Figure 1, which consists of two input/output tapers, a 3 dB MMI beam splitter (BS) and a polarization beam splitter (PBS). The silicon layer thickness of the wafer is 340 nm, and the cross-sectional width of the single-mode waveguide is 500 nm. The optical field is generated from a fiber coupled grating transmitting to the input port of 10 μm width waveguide taper coupled to a 2 μm width, and it distributes in the fundamental TE/TM mode. Then, a phase shifter and 2-2 directional couplers ensure the interference. When a single photon or weak coherent pulse is incident, the probability of output in Ch1 and Ch2 is equal.

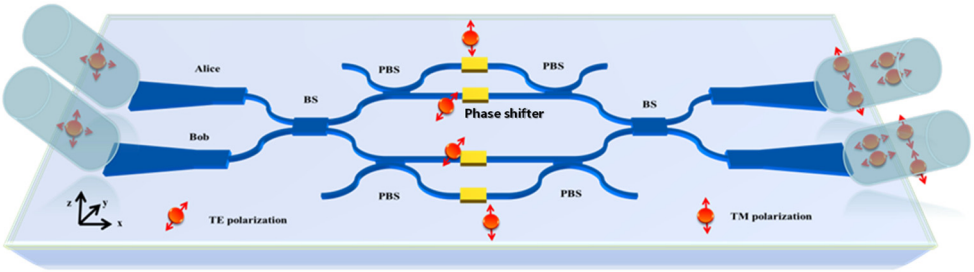

Figure 1. A schematic of the proposed interferometer structure.

For the typical waveguide taper structure [29], the incident light transmits from the 10 μm wide waveguide into the single-mode 0.5 μm wide waveguide. Then, the optical field is separated into two single-mode waveguides through a 3 dB beam splitter. The overall footprint is more than 400 μm. In this paper, we convert the fundamental TE/TM mode (TE_0/TM_0) to the first-order TE/TM mode (TE_1/TM_1) within a 10 μm wide field. Utilizing the multimode waveguide, the optical filed of the first-order mode converts to the TE_0 mode into a single-mode waveguide according to the self-imaging principle of the multimode waveguide [30]. All simulations are performed using the commercially available Finite-Difference Time-Domain (FDTD) software (version: 2020R2).

The proposed waveguide taper and beam splitters are designed following the Fermat principle and the self-imaging principle. The Fermat principle determines the length of the ladder-shaped waveguide taper of 10 μm to 2 μm. The effective refractive of incident is affected by the size of the waveguide devices, which will change the transmission path of the incident. Therefore, when the basic angle of a waveguide taper is smaller, the change in the effective refractive index is more apparent. The TE_0/TM_0 mode is converted to the 10 μm wide TE_1/TM_1 mode through a waveguide with a length of 20 μm, following the principle of phase compensation. We take the TE_1/TM_1 mode as the input and incident into the multimode interferometer couplers (MMI). Then, the high-order modes are similar to the stable mode in the single-mode waveguide, which makes arbitrary energy redistribution possible. When the MMI has input guides at the center, called symmetric interference, the length of the MMI section can be defined as follows [31]:

$$L = \frac{M}{4N} \cdot 3L_\pi \tag{1}$$

where N and $M \geq 1$ are integers and N is the number of the images. In order to reduce the length of the MMI waveguide, M is usually determined to be $M = 1$. The beat length L_π of the fundamental mode and the first-order mode are given by:

$$L_\pi = \frac{\pi}{\beta_0 - \beta_1} \tag{2}$$

$$\beta_i = \frac{2\pi}{\lambda} N_{eff}^i \tag{3}$$

where β_0 and β_1 denote the propagation constant of TE_0/TM_0, TE_1/TM_1, respectively; λ is the incident wavelength; and N_{eff}^i (i = 0, 1) is the effective refractive index of incident wavelength λ in the waveguide for TE_0/TM_0, TE_1/TM_1. The design of a polarization-independent MMI power splitter may be achieved by adjusting various parameters of the waveguide to make the L_π values of the TE and TM modes in the multimode equal to each other. That is, $\Delta\beta_{TE} = \Delta\beta_{TM}$, where $\Delta\beta_{TE}$ and $\Delta\beta_{TM}$ are the difference between β_0 and β_1 for the TE and TM mode. The parameters of the SOI waveguide under the following analysis are refractive indices of the high- and low-index regions and are 3.46 (Si) and 1.444 (SiO_2) at the wavelength of 1.55 μm, respectively. According to the self-image theory, the length, width and gap of the multimode of the beam splitter are 4 μm, 2 μm and 0.5 μm, respectively. Based on the optimized height of 340 nm, the simulated transmissions with multimode waveguide lengths, widths and wavelengths between output waveguides as degrees of freedom are shown in Figure 2a–c.

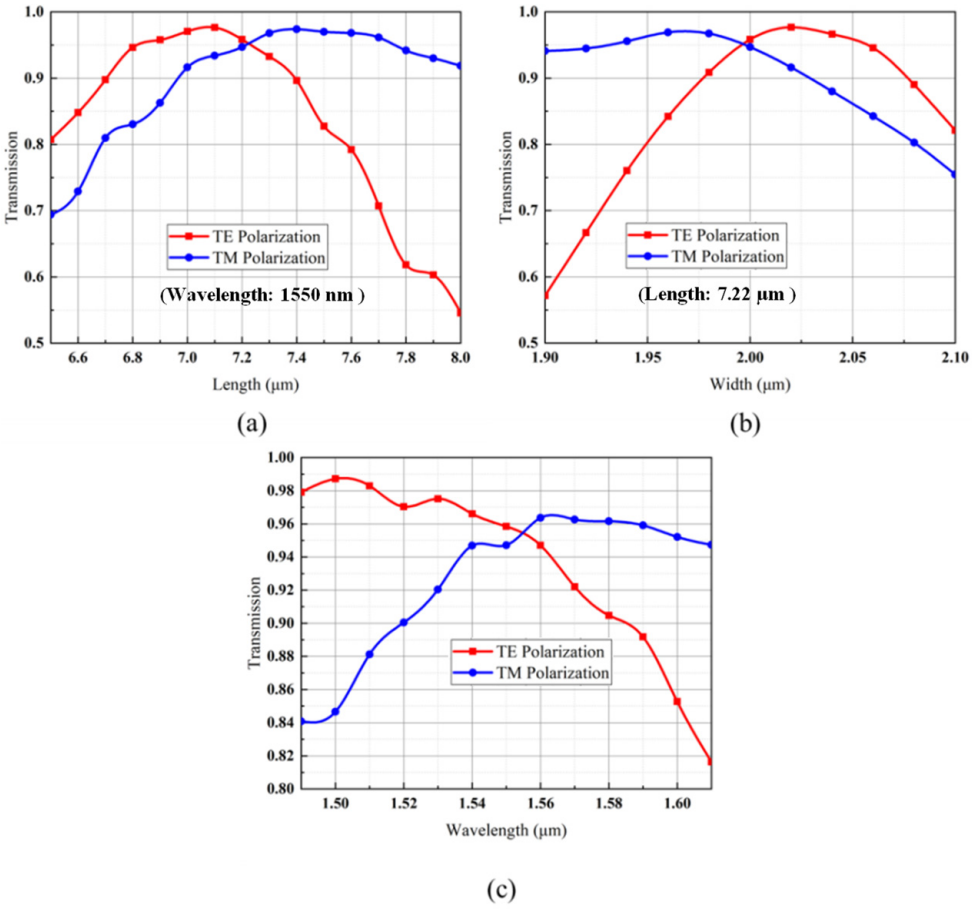

Figure 2. The transmission of beam splitters versus (**a**) MMI length, (**b**) MMI width and (**c**) wavelength. TE polarization: red solid line; TM polarization: blue solid line.

Figure 2a shows the transmission versus multimode waveguide length with a width of 2 μm and an operating wavelength at 1.55 μm. At the range of 6.7 μm to 7.6 μm, the proposed waveguide taper enables high transmission exceeding 80% for both TE and TM polarizations; meanwhile, the approximately high transmission of TE polarization (95.85%) and TM polarization (94.12%) take place at a length of 7.2 μm. The polarization dependence loss (PDL) is 0.07 dB. Therefore, the optimized length of the multimode waveguide for the proposed waveguide taper is 7.2 μm, and the total length of the proposed taper is shortened to 27.2 μm, which is one order of magnitude smaller than the reported traditional structure, with a length of 400 μm. The proposed structure at this length significantly improves the integration of the photonics integrated circuit and indicates an effective solution for potential applications in compactly high-dimensional chip-based quantum optical systems. The width of the MMI of the proposed taper is a key parameter for the design structure. Figure 2b shows the transmission versus MMI width, with a length of 7.2 μm and a wavelength of 1.55 μm. At the range of 1.95 μm to 2.1 μm, the transmission is more than 80% for both polarizations. The structure indicates polarization independence at a width of 2 μm. Additionally, based on optimized geometric dimensions (MMI length of 7.2 μm and width of 2 μm), Figure 2c describes the operated wavelength width. The transmission is more than 80% for TE and TM polarizations with a bandwidth of 120 nm (from 1.49 μm to 1.61 μm). The highest transmission of 96% for TE polarization and TM polarizations take place at wavelengths of 1.54 μm and 1.56 μm, respectively; meanwhile the 0 PDL takes place at around 1.55 μm. The transmission of proposed structure is more than 95% with a 1 dB band width of 100 nm.

The beam splitters are also designed using symmetric interference. According to Equations (1)–(3), when the MMI width is 1.76 μm, $\Delta\beta_{TE}$ equals $\Delta\beta_{TM}$, and the first-order focus is at the MMI length of 6μm for TE and TM polarizations. Next, three MMI lengths of 6 μm, 12 μm and 18 μm that correspond to the focusing orders of $M = 1$, $M = 2$ and $M = 3$, respectively, are introduced to exert the phase shift from 0° to 90° in Ch1, which determines the output port of photons in Figure 1. Figure 3 shows the electric field distributions with a phase shift of 0° and 90° for TE and TM polarizations, respectively. When $M = 1, 2, 3$, at the phase shift of 0°, the transmissions of Ch1/Ch2 are 48.92%/48.7%, 45.72%/45.61%, 42.84%/42.8% for TE polarization and 49.17%/48.84%, 48.40%/48.45%, 48.42%/47.92% for TM polarization, respectively. At the phase shift of 90°, the transmission of Ch1/Ch2 is 9.33%/74.86%, 85.91%/0.87%, 27.31%/64.16% for TE polarization and 16.96%/78.87%, 96.28%/0.83%, 19.68%/76.23% for TM polarization, respectively. The MMI lengths corresponding to $M = 1$ and $M = 3$ suffer from incomplete inter-mode coupling between fundamental modes and first-order modes, which will increase the bit error rate of the QKD systems. Due to the trade-off between efficient inter-mode coupling and low transmission loss, the optimized focusing order should be $M = 2$. Figure 4a shows the transmission versus the length of two orders focusing from 11 μm to 12.5 μm. When the MMI length reaches12.7 μm, the value of the polarization-dependent loss is lowest, and the transmissions of Ch1/Ch2 are 49.87%/49.81% and 49.07%/49.06%. The transmission versus with the wavelength is shown in Figure 4b. The highest transmissions of 0.49879/0.49814 and 0.49156/0.49133 for TE polarization and TM polarization take place at wavelengths of 1.55 μm and 1.56 μm, respectively. Meanwhile, the zero PDL takes place at the wavelength of 1.56 μm and the highest visibility of our design interferometer is 99.65% and 98.70% for TE and TM polarization, respectively, as shown in Figure 5a,b.

3dB MMI coupler design:

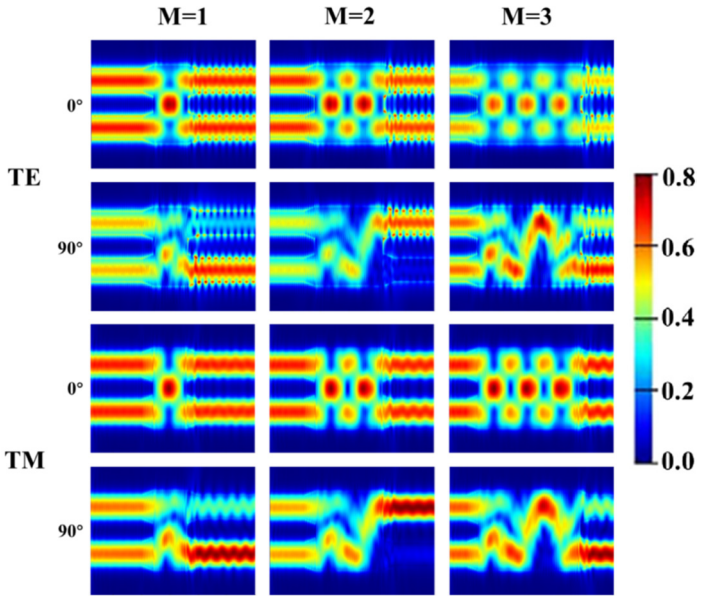

Figure 3. The electric field distribution with phase shifts of 0 and 90 degrees for M = 1, 2 and 3.

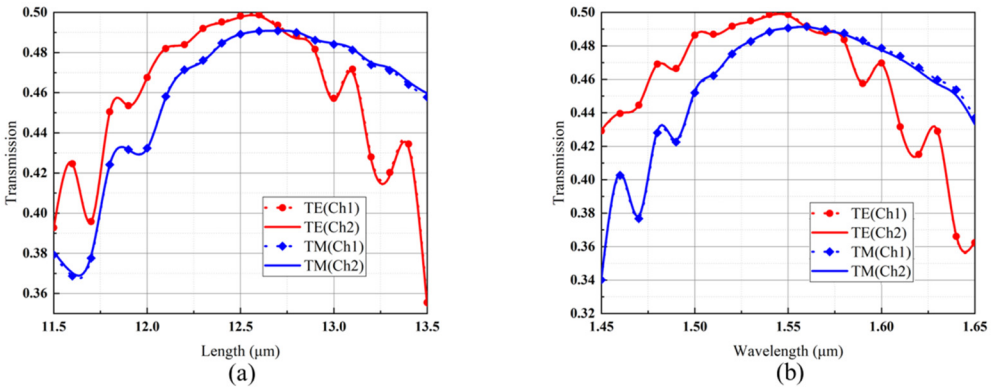

Figure 4. The transmission of 3 dB MMI beam splitters versus (**a**) MMI length and (**b**) wavelength. TE polarization and Ch1: red circle; TE polarization and Ch2: red solid line; TM polarization and Ch1: blue diamond; TM polarization and Ch2: blue solid line.

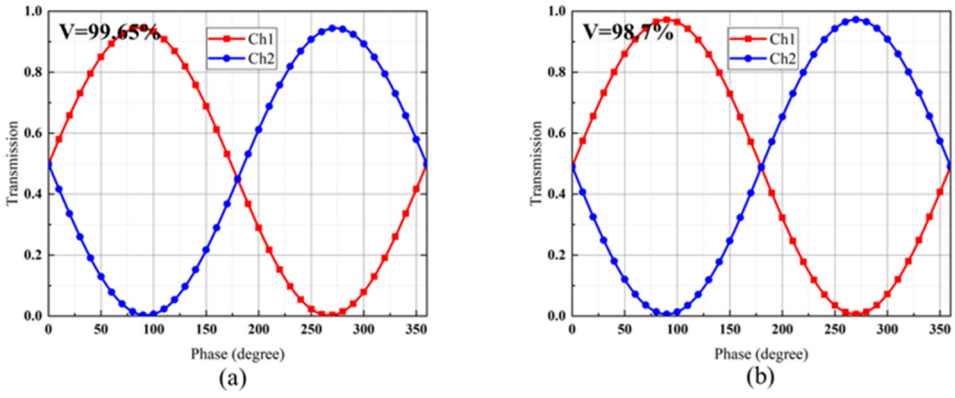

Figure 5. The normalized transmittance versus phase shift added in Ch1 for (**a**) TE polarization and (**b**) TM polarization.

The Polarization Beams Splitters Design

The polarization beams splitters are designed using anisotropic metamaterials cladding, which can suppress the couplings for TE polarization. The anisotropic metamaterials are composed of sub-wavelength multilayer claddings with a period of T = 100 nm, a fill factor f = 0.5 and a period number N = 2. By carefully designing the coupling length, we propose an ultra-short directional coupler which can separate the TE and TM polarization fields thanks to the different refractive indices between TE and TM polarization. When a mixed-polarized field incident comes from the TRU port, the TE polarization passes through, while the TM polarization couples into the other CUO port. To optimize the DC, we analyzed the influence of the coupling length on the transmission for TM polarization, which reaches 98%, while for TE polarization, it is only 0.69%, resulting in an extinction ratio of 21 dB. On the other hand, at length of 10.7 μm, the extinction ration achieves 22 dB at Ch1, where the transmission of TE polarization is 98% and 0.59%. Hence, TE and TM polarizations can be separated by the designed directional couplers with a high efficiency and low crosstalk at an ultra-short coupling length of 10.7 μm. According to Figure 6a, an extinction ratio above 20 dB is achieved in both channels with a large coupling length fabrication tolerance of 0.5 μm (10.6–11.1 μm). The transmission versus with the wavelength is shown in Figure 6b. A 100 nm 1 dB bandwidth of incident spectrum ranging from 1.51 to 1.6 μm can be observed. The highest efficiency of 98% and PER of 23 dB for both polarizations take place at a wavelength λ = 1.56 μm. The simulated electric field distribution for TE and TM polarization are shown in Figure 6c. The operation wavelength λ = 1.56 μm, and corresponding refractive index for Si and SiO_2 are 3.46 and 1.444, respectively. The TE polarization incident is transmitted directly into the TRU port, and TM polarizations are coupled from the TRU port to the CUO port due to the phase matching. From the profiles, the residual power for TE/TM polarization could be negligible in the CUO/TRU ports. The simulations present a structure design for bi-polarizations PBSs with transmissions over 98%, which provides a potential optical router for a quantum communication system. It should be noted that the back-reflection effects at the input and output of the device, the losses in the single-photon detection processes and the quantum bit error rate should be considered in the related quantum communication system's design [32].

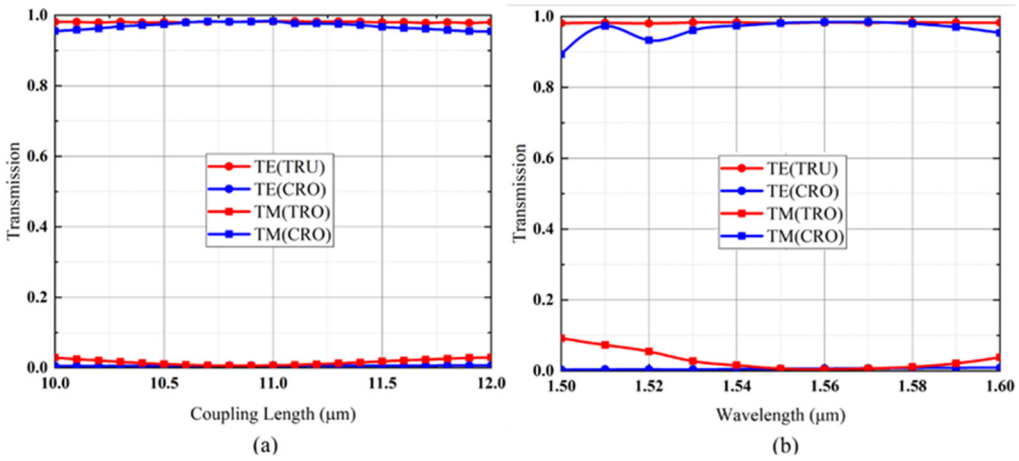

Figure 6. *Cont.*

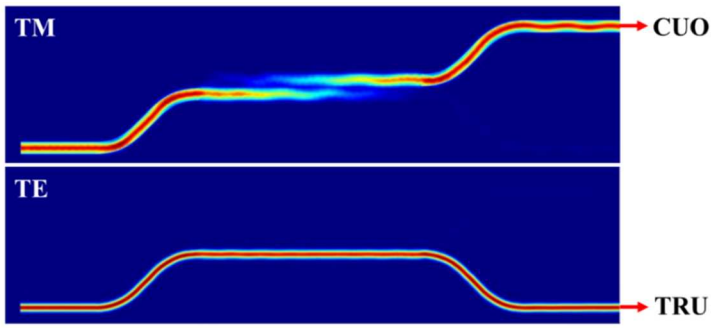

Figure 6. (**a**) and (**b**) are the transmission of PBS versus coupler length and wavelength, respectively, and (**c**) is the electric distribution in PBS.

3. Discussion

3.1. Single-Photon State Conversion [33]

A single photon sent to Alice is transformed into a superposition across modes by the 3 dB coupler:

$$|\psi\rangle = (|1\rangle_A|0\rangle_B + |0\rangle_A|1\rangle_B)/\sqrt{2} \tag{4}$$

The photon for TE polarization transmits directly along path 2 or path 3 and is controlled by the relative optical phase ϕ_1. The TM polarization transmission is coupled by the PBS and transmits along path 1 or path 4 and is controlled by the relative optical phase ϕ_2. The single-photon state for both polarizations can be described by:

$$|\psi\rangle_{TE} = \left(|1\rangle_2|0\rangle_3 + ie^{\phi_2}|0\rangle_2|1\rangle_3\right)/\sqrt{2} \tag{5}$$

$$|\psi\rangle_{TM} = \left(|1\rangle_1|0\rangle_4 + ie^{i\phi_1}|0\rangle_1|1\rangle_4\right)/\sqrt{2} \tag{6}$$

By modulating the phase, TE and TM polarized light could be output from a fixed port, Alice or Bob. When $\phi_1 = \phi_2 = 90^\circ$, the MZI structure is equivalent to a 3 dB beam splitter, and the single photon is still in the quantum superposition state, as shown in Equation (1). When $\phi_1 = 180^\circ$, $\phi_2 = 0^\circ$, the TE and TM polarized photons output at Alice's and Bob's ports, respectively. In this part, the photon state encodes by path converted to polarization:

$$|\psi\rangle = (|1\rangle_{TE}|0\rangle_{TM} + |0\rangle_{TE}|1\rangle_{TM})/\sqrt{2} \tag{7}$$

The above analysis shows that we can achieve arbitrary conversion of single photon coding between path and polarization degree of freedom by controlling the relative phases of ϕ_1 and ϕ_2, respectively.

3.2. Polarized Entangled Photon Pairs [34]

The photon source generates polarized entangled photon pairs; one is sent to Alice and the other is sent to Bob simultaneously by the structure in Figure 1. Suppose that Alice and Bob share N photon pairs in the following entangled states:

$$|\psi\rangle = (|H\rangle_A|H\rangle_B + |V\rangle_A|V\rangle_B)/\sqrt{2} \tag{8}$$

The single photons with the same polarization denoted as the $|\psi\rangle = |1\rangle_A|1\rangle_B$ state are subject to interference from the 3 dB coupler and generate a two-photon quantum NOON state, encoded by the path as

$$|\psi\rangle_{TE/TM} = (|2\rangle_A|0\rangle_B + |0\rangle_A|2\rangle_B)/\sqrt{2} \tag{9}$$

The PBS acts as a multiplexer which couples the photons for TM polarization from the one path to the other path without affecting TE-polarized photons. So, the states of $|\psi\rangle_{TM} = |0\rangle_A|2\rangle_B$ and $|\psi\rangle_{TM} = |2\rangle_A|0\rangle_B$ are coupled to path A and path B, respectively. The in-paths A and B generate a polarization encoding the NOON entanglement state:

$$|\psi\rangle = (|2\rangle_{TE}|0\rangle_{TM} + |0\rangle_{TE}|2\rangle_{TM})/\sqrt{2} \quad (10)$$

where the path encoding state converts to the polarization encoding state and can transmit to different users that are available for quantum precision measurement, quantum computation and HOM experiments.

4. Conclusions

In summary, we propose and numerically simulate an MZI-based active bi-polarization QR for the generation of photon-entangled states and the conversion between quantum states. The proposed QR can realize dual path polarization conversion on an SOI platform. The length of the waveguide taper is shortened by an order of magnitude, with transmissions beyond 95% for both TE and TM polarizations, utilizing the principle of phase compensation and self-image. Using anisotropic metamaterials, the polarization beam splitter is optimized to have an ultra-compact footprint of 1.4×10.4 μm^2 with transmissions of 98% for bi-polarizations. The proposed ultra-compact QR shows the advantages of low loss, a broad operating spectral range and a large tolerance to size variation in fabrications. It is anticipated to find promising applications in the fields of integrated quantum photonic circuits, quantum secure direct communication [35] and studying fundamental properties of physics [36].

Author Contributions: Writing—original draft preparation, Z.D.; data curation, Z.D. and E.P.; software, Z.D., E.P. and X.C.; validation, X.C. and X.S.; writing—review and editing, H.Z.; supervision, Y.L. All authors have read and agreed to the published version of the manuscript.

Funding: This research was funded by the National Natural Science Foundation of China (62205131, 62005107, 62005074); the Natural Science Research Project of Higher Education Institutions of Jiangsu Province (22KJB140002); the Natural Science Foundation of Jiangsu Province (BK20220519, BK20221363); the China Postdoctoral Fund (2022M721378); and the State Key Laboratory of Infrared Physics, Shanghai Institute of Technical Physics, Chinese Academy of Sciences (Grant No. SITP-NLIST-YB-2022-13).

Institutional Review Board Statement: Not applicable.

Informed Consent Statement: Not applicable.

Data Availability Statement: Data are contained within the article.

Conflicts of Interest: The authors declare no conflict of interest.

References

1. MacQuarrie, E.R.; Simon, C.; Simmons, S.; Maine, E. The emerging commercial landscape of quantum computing. *Nat. Rev. Phys.* **2020**, *2*, 596–598. [CrossRef]
2. Yuan, H.Y.; Cao, Y.; Kamra, A.; Duine, R.A.; Yan, P. Quantum magnonics: When magnon spintronics meets quantum information science. *Phys. Rep.* **2022**, *965*, 1–74. [CrossRef]
3. Stas, P.J.; Huan, Y.Q.; Machielse, B.; Knall, E.N.; Suleymanzade, A.; Pingault, B.; Sutula, M.; Ding, S.W.; Knaut, C.M.; Assumpcao, D.R.; et al. Robust multi-qubit quantum network node with integrated error detection. *Science* **2022**, *378*, 557–560. [CrossRef] [PubMed]
4. Chen, Y.A.; Zhang, Q.; Chen, T.Y.; Cai, W.-Q.; Liao, S.-K.; Zhang, J.; Chen, K.; Yin, J.; Ren, J.-G.; Chen, Z.; et al. An integrated space-to-ground quantum communication network over 4600 kilometres. *Nature* **2021**, *589*, 214–219. [CrossRef]
5. Bassoli, R.; Boche, H.; Deppe, C.; Ferrara, R.; Fitzek, F.H.P.; Janssen, G.; Saeedinaeeni, S. *Quantum Communication Networks*; Springer: Berlin/Heidelberg, Germany, 2021.
6. O'Brien, J.L.; Furusawa, A.; Vukovi, J. Photonic quantum technologies. *Nat. Photonics* **2010**, *3*, 687–695. [CrossRef]
7. Wang, M.; Wu, R.; Lin, J.; Zhang, J.; Fang, Z.; Chai, Z.; Cheng, Y. Chemo-mechanical polish lithography: A pathway to low loss large-scale photonic integration on lithium niobate on insulator. *Quantum Eng.* **2019**, *1*, e9. [CrossRef]

8. Wang, R.; Sprengel, S.; Muneeb, M.; Boehm, G.; Baets, R.; Amann, M.-C.; Roelkens, G. 2 µm wavelength range InP-based type-II quantum well photodiodes heterogeneously integrated on silicon photonic integrated circuits. *Opt. Express* **2015**, *23*, 26834–26841. [CrossRef]
9. Poot, M.; Schuck, C.; Ma, X.-S.; Guo, X.; Tang, H.X. Design and characterization of integrated components for SiN photonic quantum circuits. *Opt. Express* **2016**, *24*, 6843–6860. [CrossRef]
10. Zhang, J.; Shi, X.; Zhang, Z.; Guo, K.; Yang, J. Ultra-compact, efficient and high-polarization-extinction-ratio polarization beam splitters based on photonic anisotropic metamaterials. *Opt. Express* **2022**, *30*, 538–549. [CrossRef]
11. Awschalom, D.; Berggren, K.K.; Bernien, H.; Bhave, S.; Carr, L.D.; Davids, P.; Economou, S.E.; Englund, D.; Faraon, A.; Fejer, M.; et al. Development of Quantum Interconnects (QuICs) for Next-Generation Information Technologies. *PRX Quantum* **2021**, *2*, 017002. [CrossRef]
12. Lee, Y.; Bersin, E.; Dahlberg, A.; Wehner, S.; Englund, D. A quantum router architecture for high-fidelity entanglement flows in quantum networks. *npj Quantum Inf.* **2022**, *8*, 75. [CrossRef]
13. Cao, C.; Han, Y.H.; Yi, X.; Yin, P.-P.; Zhang, X.-Y.; Gao, Y.-P.; Fan, L. Implementation of a single-photon fully quantum router with cavity QED and linear optics. *Opt. Quantum Electron.* **2021**, *53*, 32. [CrossRef]
14. Xia, K.; Jelezko, F.; Twamley, J. Quantum routing of single optical photons with a superconducting flux qubit. *Phys. Rev. A* **2018**, *97*, 052315. [CrossRef]
15. Shou, C.; Zhang, Q.; Luo, W.; Huang, G. Photon storage and routing in quantum dots with spin-orbit coupling. *Opt. Express* **2021**, *29*, 9772–9785. [CrossRef] [PubMed]
16. Childress, L.; Hanson, R. Diamond NV centers for quantum computing and quantum networks. *Mrs Bull. Mater. Res. Soc.* **2013**, *38*, 134–138. [CrossRef]
17. Matthews, J.; Politi, A.; Stefanov, A.; O'Brien, J.L. Manipulating multi-photon entanglement in waveguide quantum circuits. *Nat. Photonics* **2009**, *3*, 346–350. [CrossRef]
18. Zhang, G.; Haw, J.Y.; Cai, H.; Xu, F.; Assad, S.M.; Fitzsimons, J.F.; Zhou, X.; Zhang, Y.; Yu, S.; Wu, J.; et al. An integrated silicon photonic chip platform for continuous-variable quantum key distribution. *Nat. Photonics* **2019**, *13*, 839–842. [CrossRef]
19. Kwek, L.C.; Cao, L.; Luo, W.; Wang, Y.; Sun, S.; Wang, X. Chip-based quantum key distribution. *AAPPS Bull.* **2021**, *31*, 15. [CrossRef]
20. Lu, L.; Xia, L.; Chen, Z.; Chen, L.; Yu, T.; Tao, T.; Ma, W.; Pan, Y.; Cai, X.; Lu, Y.; et al. Three-dimensional entanglement on a silicon chip. *npj Quantum Inf.* **2020**, *6*, 30. [CrossRef]
21. Qiang, X.; Loke, T.; Montanaro, A.; Aungskunsiri, K.; Zhou, X.; O'Brien, J.L.; Wang, J.B. Efficient quantum walk on a quantum processor. *Nat. Commun.* **2016**, *7*, 11511. [CrossRef]
22. Zhang, M.; Feng, L.; Li, M.; Chen, Y.; Zhang, L.; He, D.; Guo, G.; Guo, G.; Ren, X.; Dai, D. Supercompact Photonic Quantum Logic Gate on a Silicon Chip. *Phys. Rev. Lett.* **2021**, *126*, 130501. [CrossRef] [PubMed]
23. Ding, Y.; Bacco, D.; Dalgaard, K.; Cai, X.; Zhou, X.; Rottwitt, K. High-dimensional quantum key distribution based on multicore fiber using silicon photonic integrated circuits. *npj Quantum Inf.* **2017**, *3*, 25. [CrossRef]
24. Wang, J.; Bonneau, D.; Villa, M.; Silverstone, J.W.; Santagati, R.; Miki, S.; Yamashita, T.; Fujiwara, M.; Sasaki, M.; Terai, H.; et al. Chip-to-chip quantum photonic interconnect by path-polarization interconversion. *Optica* **2016**, *3*, 407–413. [CrossRef]
25. Xie, Z.; Tian, Z.; Shrestha, S.; Xu, X.; Liang, J.; Gong, Y.-X.; Bienfang, J.C.; Restelli, A.; Shapiro, J.H.; Wong, F.N.C.; et al. Harnessing high-dimensional hyperentanglement through a biphoton frequency comb. *Nat. Photonics* **2015**, *9*, 536. [CrossRef]
26. Ma, C.; Sacher, W.D.; Tang, Z.; Mikkelsen, J.C.; Yang, Y.; Xu, F.; Thiessen, T.; Lo, H.-K.; Poon, J.K.S. Silicon photonic transmitter for polarization-encoded quantum key distribution. *Optica* **2016**, *3*, 1274–1278. [CrossRef]
27. Zhong, T.; Zhou, H.; Horansky, R.D.; Lee, C.; Verma, V.B.; Lita, A.E.; Restelli, A.; Bienfang, J.C.; Mirin, R.P.; Gerrits, T.; et al. Photon-efficient quantum key distribution using time–energy entanglement with high-dimensional encoding. *New J. Phys.* **2015**, *17*, 022002. [CrossRef]
28. Long, G.L. General quantum interference principle and duality computer. *Commun. Theor. Phys.* **2006**, *45*, 825.
29. Burns, W.K.; Milton, A.F.; Lee, A.B. Optical waveguide parabolic coupling horns. *Appl. Phys. Lett.* **1977**, *30*, 28–30. [CrossRef]
30. Chen, X.F.; Shi, X.D.; Qiu, P.F.; Dai, Z.J.; Yu, Y.; Song, X.X.; Zhang, H.T.; Chen, M.Y.; Ye, Y.X.; Ren, X.D.; et al. Efficient mode converters and filters using asymmetrical directional couplers with subwavelength gratings. *Opt. Lett.* **2022**, *47*, 4600–4603. [CrossRef]
31. Mia, M.B.; Ahmed, S.Z.; Ahmed, I.; Lee, Y.J.; Qi, M.; Kim, S. Exceptional coupling in photonic anisotropic metamaterials for extremely low waveguide crosstalk. *Optica* **2020**, *7*, 881–887. [CrossRef]
32. Simmons, C.; Donaldson, R. Multicore fiber beacon system for reducing back-reflection in satellite quantum key distribution. *Opt. Express* **2023**, *31*, 23382–23392. [CrossRef] [PubMed]
33. O'Connor, D. *Time-Correlated Single Photon Counting*; Academic press: Cambridge, MA, USA, 2012.
34. Orieux, A.; Versteegh, M.A.M.; Jöns, K.D.; Ducci, S. Semiconductor devices for entangled photon pair generation: A review. *Rep. Prog. Phys.* **2017**, *80*, 076001. [CrossRef] [PubMed]

35. Long, G.L.; Liu, X.S. Theoretically efficient high-capacity quantum-key-distribution scheme. *Phys. Rev. A* **2002**, *65*, 032302. [CrossRef]
36. Wang, Y.; Yu, X.; Xue, S.; Wang, Y.; Zhan, J.; Wu, C.; Zhu, P.; Zheng, Q.; Yu, M.; Liu, Y.; et al. Experimental demonstration of quantum transport enhancement using time-reversal symmetry breaking on a silicon photonic chip. *Sci. China Phys. Mech. Astron.* **2022**, *65*, 100362. [CrossRef]